ADVANCES IN FOREST FIRE RESEARCH

2022

Edited by
DOMINGOS XAVIER VIEGAS
LUÍS MÁRIO RIBEIRO

Influence of a sea-breeze front over a fire plume, Pedrogão Grande wildfires (20 June 2017)

Paulo Pinto*[1]; Álvaro Silva[1]; Domingos Viegas[2], Miguel Almeida[2], Luís Mário Ribeiro[2]

[1] Portuguese Institute for Sea and Atmosphere (IPMA), Rua C do Aeroporto, 1749-077 Lisbon, Portugal, {paulo.pinto, alvaro.silva@ipma.pt}
[2]Forest Fire Research Centre. University of Coimbra, ADAI, Department of Mechanical Engineering, Rua Luís Reis Santos, Pólo II, 3030-788 Coimbra, Portugal., {miguelalmeida, luis.mario}@adai.pt, xavier.viegas@dem.uc.pt

**Corresponding author*

Keywords

Sea-breeze front, pyroCumulus, weather radar, Dual-polarization

Abstract

During the afternoon of 20 June 2017, two massive wildfires were ongoing more than 30 km to the east-southeast of the city of Coimbra, central Portugal. There were no clouds over the location and surrounding areas. As these fires were progressing, smoke plumes were observed with their tops at around 6-7 km a.m.s.l. However, as a sea-breeze front arrived at the buoyancy sources it was observed an outstanding vertical growth of the plumes. One of these developments was particularly analyzed and it was found that the plume topped at nearly double that altitude in less than 60 min. As a result of this interaction, an impressive pyroCumulus cloud formed. This process was analyzed using weather radar with Dual polarization capabilities.

1. Introduction

The fire complex of Pedrogão Grande, during 17-22 June 2017, was considered as the worst on record in Portugal due to the large burnt area and related fatalities, as described in Viegas et al. (2017). The influence of a mesoscale convective system over the fires was analyzed in Pinto et al. (2022) for an event of 17 June.

Further from convective flows induced by meteorological systems, the progression of sea-breeze fronts (SBF's) over fire areas has also been described as an important mechanism of interaction with smoke plumes, generating transient, though significant, increase in fire intensity, as discussed by Hanley et al (2013). A SBF is the outcome of a thermally-driven mesoscale circulation that results from the differential heating over land and oceanic bodies. During the day, warmer and less dense air over land generates lower air pressure than over the ocean where cooler, denser air, resides. As a result, the mesoscale front propagates inland as the cooler air flows towards land to replace warmer air. These phenomena are known to trigger convection inland, as increased low-level convergence lifts the air and facilitates moisture convergence, Pielke et al. (1991). As a SBF propagates over a location, air moisture usually increases, temperature drops, wind direction may suddenly shift, gusts may be produced and air quality may also change, as shown by Miller et al. (2003). Coupled atmosphere-fire models are required to understand, in detail, the interaction between SBF's and the fires, as pointed out by Hanley et al (2013). However, the monitoring of the interaction between the SBF and the pyroconvective plume may suggest important impacts on the fire. During the afternoon of 20 June, a SBF was observed to propagate across the area where two fires were progressing.

2. Sea-breeze front

2.1. Numerical Weather analysis and forecast

At 12:00 (all times are UTC) of 20 June 2017, the UK Met Office mean sea-level pressure analysis showed a low to the west of Portugal and an anticyclone over central Mediterranean that was promoting the advection of a hot and dry airmass over western Iberia (Figure 1a). Over central Portugal the low-level flow was weak from the east-southeast, inland, and also light, but from the west-northwest along the coast as shown by the 12:00

ECMWF forecast (Figure 1b). Above 500 hPa (5900 m a.m.s.l.), at 12:00, the flow was from the west according to the rawinsonde from Lisbon (Figure 2). The sounding also showed an inverted-V type profile with relatively moist air in the 700-600 hPa layer but a dry airmass below 700 hPa (Figure 2). This typical profile has been referred in pyrocloud case studies such as Fromm et al. (2012) and Peterson et al. (2017).

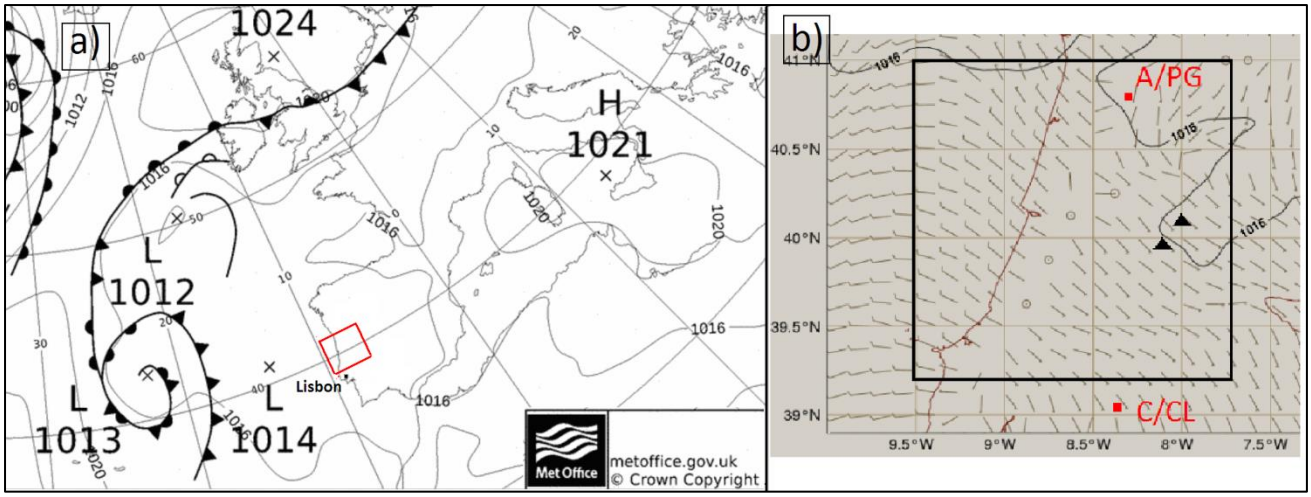

Figure 1- (a) Mean sea-level pressure analysis (solid contours, 4-hPa intervals) over the Northeast Atlantic (adapted from Uk Met Office), red square defines area in (b), Lisbon sounding station represented by a dot and (b) Zoomed-in area from (a) 10 m wind speed and direction (wind barbs notation) over mainland Portugal, ECMWF forecast H+12, black square defines central Portugal, A/PG and C/CL radars are represented by a red square symbol and fire locations are represented by black triangles, 12:00 UTC, 20 June 2017.

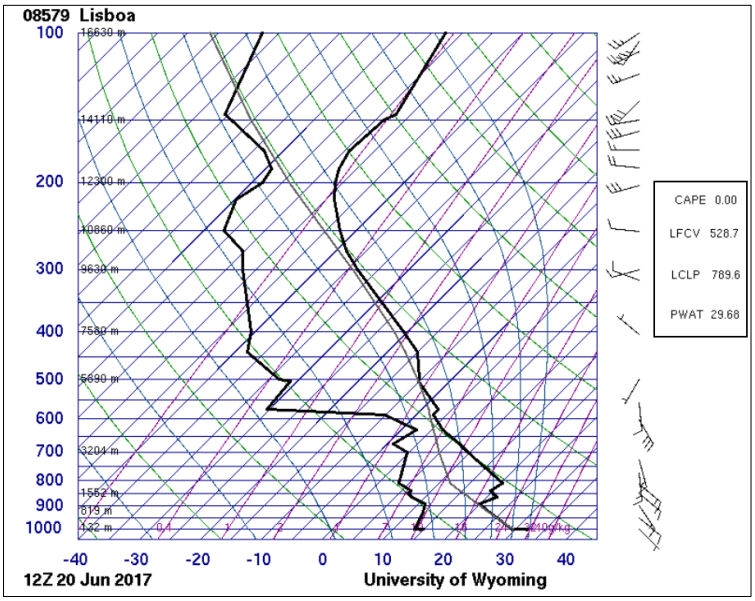

Figure2- Skew-T chart for rawinsonde profile for Lisboa station (08579) at 12:00 UTC, 20 June 2017 (location is indicated in Figure 1a). Dry bulb air temperature (black line, right), dew point temperature (black line, left), parcel trajectory (grey line, middle) and wind barbs at different levels are represented. Sounding indices: CAPE (J/Kg), LFCV (Level of free convection using virtual temperature, hPa), LCLP (Lifting condensation level, hPa) and Precipitable water for the entire sounding(8mm), adapted from University of Wyoming (http://weather.uwyo.edu/upperair/europe.html)

An area of low-level convergence (LLC) was identified to the west of the fires along a coastal strip in the 10 m wind forecast, at 12:00 (Figure 1b), coinciding with a large horizontal gradient in relative air humidity (Figure 3a). Dry air (<35%) was located to the east of the LLC whereas moister air was forecasted to the west of it (Figure 3a). Forecasts also showed that the LLC was separating warmer air to the east, from cooler air to the west, at 12:00 (not shown). Forecasts from 12:00, 15:00 and 18:00 anticipated that the LLC would propagate

eastwards, over the fires area (not shown) always separating cooler, moister air (Figure 3b,c) to its west, from warmer, drier air (Figure 3b,c) to its east. This was materializing the propagation of a SBF.

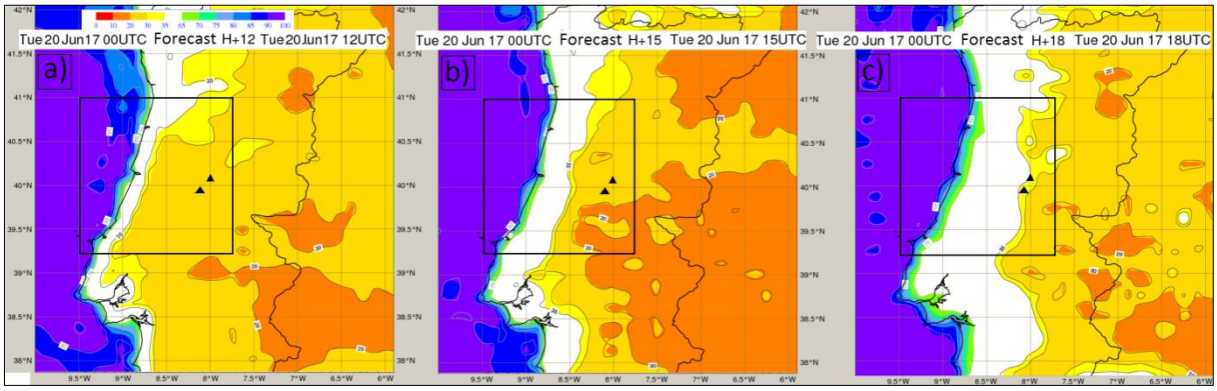

Figure 3- (a) 10 m Relative humidity (shaded, %) ECMWF forecast H+12, 12:00 UTC, (b) H+15, 15:00 UTC, and (c) H+18, 18:00 UTC, 20 June 2017. Fire locations are represented by black triangles.

2.2. Radar and surface observations

Two Doppler radars from the Instituto Português do Mar e da Atmosfera (IPMA) network were used. The Porto radar (A/PG), a dual polarization system (DP), it is located 100 km to the north of the fires (Figure 1b) and at 1100 m a.m.s.l.. The Lisbon radar (C/CL), a single polarization system (SP), it is located 100 km to the south of the fires (Figure 1b) and at 200 m a.m.s.l.. From each of the radar, reflectivity scan observations were extracted every 10 min. C/CL observations offered the best view of the low-level reflectivity due to the lower altitude of the beam, thus low elevation plane position indicators of reflectivity (PPZ) were extracted from this radar. The A/PG radar processed the correlation coefficient (ρhv) due to its DP technology.

Low-level reflectivity from C/CL radar was detected 400 m above two main active fires that were progressing in central Portugal (Figure 1b). The follow-up of reflectivity allowed the identification of the buoyancy sources (Figure 4). Visible channel satellite imagery (not shown) has confirmed that the sky was clear in the area, thus the fire plume was the only object detected on radar. Orientation of the plume and its evolution were derived from a reflectivity pattern extending downwind of the buoyancy sources (Figure 4b).

As a result of fires intensification, there is an increase in the combustion processes and in buoyancy that transport more and larger pyrometeors (McCarthy et al., 2019) upwards, according to McCarthy et al. (2019) and Jones et al. (2010). These effects will increase reflectivity (considering its dependency on the sixth power of the backscatterers diameter) and generate taller plumes. Thus, magnitude of low-level reflectivity close to the fire site and the vertical extent of the plume are good indicators of the general intensity of the strong convective processes caused by the fire (pyroconvection).

The parameter ρhv is a correlation, in a time series, between horizontally and vertically polarized echoes and is a fine particle type discriminator according to Balakrishnan et al. (1990). Lang et al. (2014), LaRoche et al. (2017) showed that fire particles exhibit ρhv values lower than those associated to hydrometeors. In accordance with Pinto et al. (2022), this study assumes that atmospheric volumes with $\rho hv \leq 0.7$ are mainly filled in by pyrometeors without significant condensation, whereas larger values correspond to atmospheric volumes with significant condensation/glaciation of pyrometeors.

Thin reflectivity lines that are traceable on radar may result from the local increase in reflectivity that is associated with the stacking of scatterers generated by low-level convergence. This can be associated with convective outflows, Srivastava et al. (1987), but also, as shown by Hanley et al (2013), with SBF's. A thin reflectivity line was identified on the lowest tilt from the C/CL scan during the afternoon of the 20 June (Figure 4).

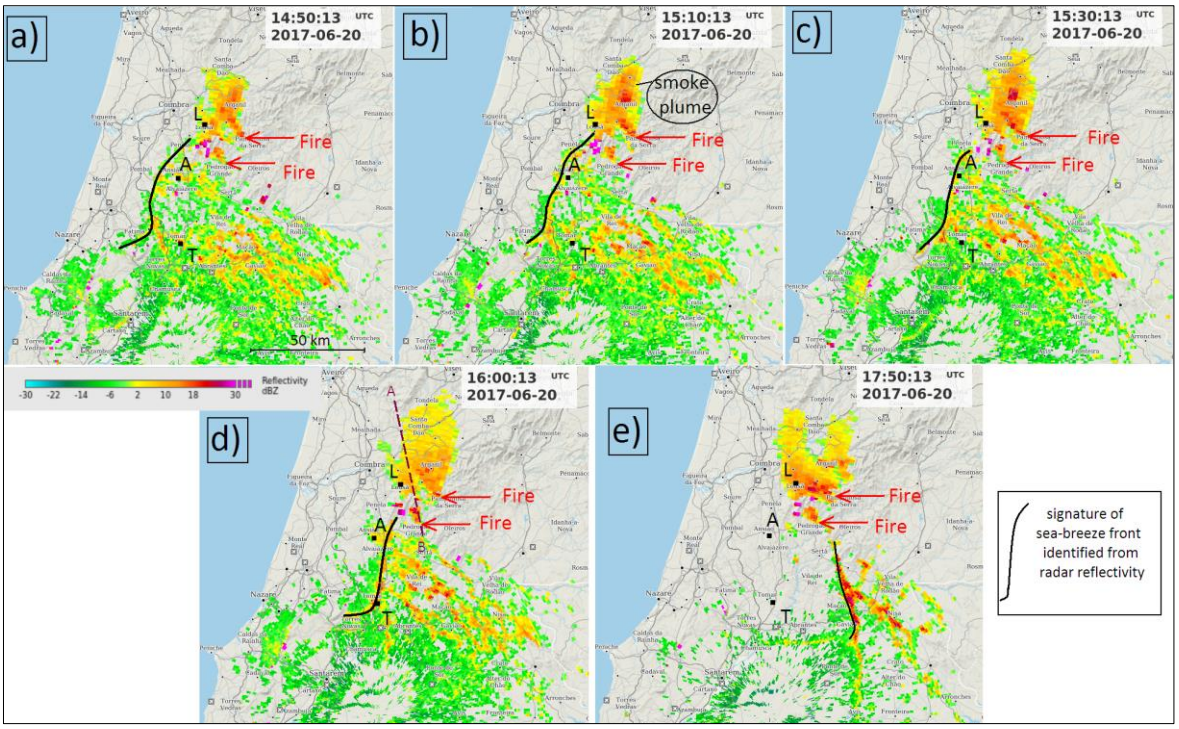

Figure 4- PPI of reflectivity, 0.1° tilt, 20 June 2017, C/CL radar. (a) 14:50 UTC, (b) 15:10 UTC, (c) 15:30 UTC, (d) 16:00 UTC, (e) 17:50 UTC. "L" Lousã, "A" Ansião, "T" Tomar AWS's. Buoyancy sources are represented by red arrows and "FIRE". "AB" dashed segment in (d) represents transect of the vertical section represented in Figure 7(a). "Smoke Plume" in a black circle in (b) highlights the pattern of a smoke plume.

The line started to be identified at 14:50, still to the west of three automatic weather stations (AWS) of IPMA (Figure 4a). Two-meter air temperature and relative humidity, 10m wind gusts and average wind speed and direction, were recorded every 10min. At this time AWS's ("L", Lousã; "A", Ansião; "T", Tomar) were influenced by a hot and dry airmass (40 °C, < 25%) and light winds from the south or southeast (Figure 5). The line was propagating eastwards and as it arrived at "L" by 15:10 the AWS started to record a decrease in air-temperature and an increase in relative humidity. However, the sudden shift to a westerly flow was the most noticeable change (Figure 5c). The other AWS's remained under the influence of a hot and dry airmass (Figure 5a,b). By 15:30, as the line arrived at "A" (Figure 4c) the AWS started to record a substantial decrease in air-temperature and increase in relative humidity (Figure 5b). It was also observed a shift to a westerly flow and average wind and gusts increment (Figure 5b). "T" AWS, still located to the east of the line (Figure 4c), remained under the influence of a dry and hot airmass in southeasterly winds (Figure 5a). At 16:00, as the thin line finally arrived at "T" (Figure 4d), the AWS recorded the same qualitative changes observed in the other AWS, concurrently with the thin line arrival (Figure 5a). By this time, the three AWS were being influenced by a cooler and moister airmass than before. These observations showed that the thin reflectivity line that was identified on low-level reflectivity was, indeed, coherently associated with the propagation of a SBF. The findings were similar to those documented by Hanley et al. (2013). This behavior confirmed the forecasts of the ECMWF and highlighted the fine performance of the model for this event (Figure 3).

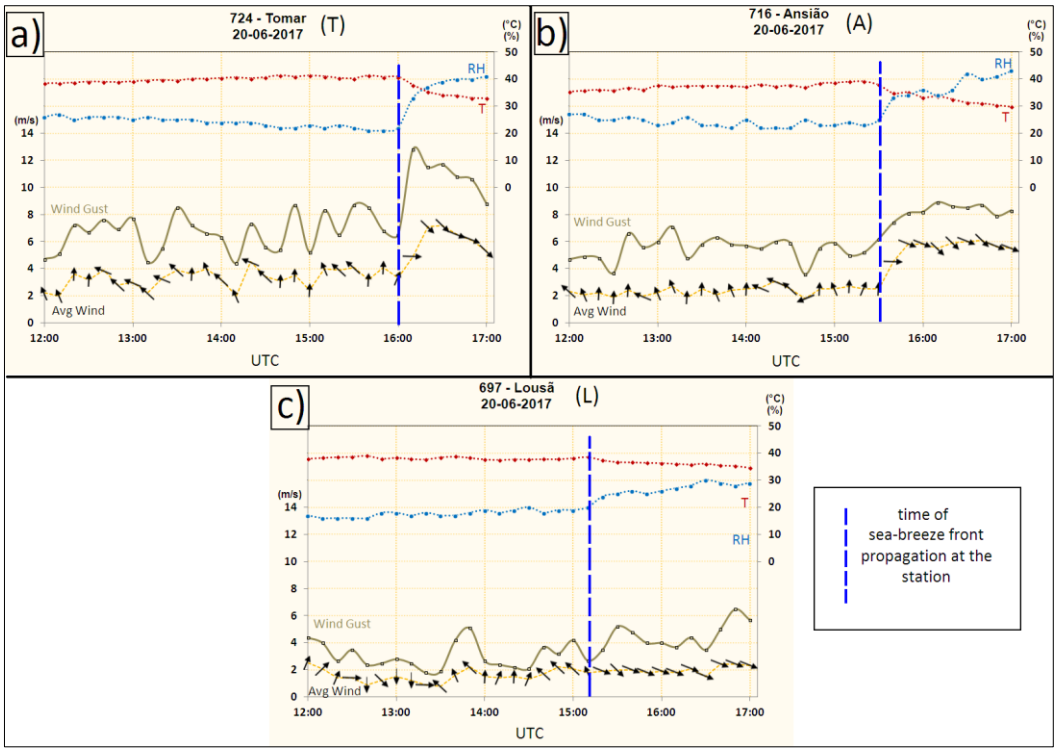

Figure 5- Weather observations at the AWS (a) Tomar ("T"), (b) Ansião ("A"), (c) Lousã ("L"). 2m air temperature (T, red), relative humidity (RH, blue), magnitude of 10 m wind gusts (green cyan), magnitude of 10 m average wind (dotted black line) and direction (arrows) observed during 12:00-17:00 UTC, 20 June 2017.

3. Influence of the sea-breeze front over the fire plume: pyroCumulus formation

The magnitude of low-level reflectivity close to buoyancy sources was monitored according to a method described in Pinto et al. (2022). The monitoring for the southwest fire (Figure 4) yielded magnitudes of 9-16 dBZ for the period 14:50-15:50 (Figure 4a,b,c). Then, from 15:50 to 16:00, an increase from 16 to 21 dBZ was noticed for this fire. At 16:10 a similar value was observed and slightly lower values were found afterwards (not shown).

Miller et al. (2003) show a diagram (their figure 9) of the simplified two-dimensional flow of a gravity current such as a SBF. Their study refers to a SBF head that may extend for more than 2000 m above the surface and explains that the flow of the pre-frontal area may promote convective activity due to the favored vertical motions. On this concern Hanley et al. (2013) have noticed that the reflectivity of a smoke plume increased substantially when a SBF was approaching the fire, but still 5-7 km upwind of it (their Figure 7.3) and considered that this was the result of enhanced low-level convergence and vertical motion ahead of the front.

The increase observed in reflectivity at 16:00, however seeming small in dBZ units, it equates to a large difference in base linear reflectivity units, since the factor is logarithmic due to its dependency on the sixth power of the scatterers diameter. Thirty minutes before this increase has occurred, the SBF was 15 km to the west of the buoyancy source (Figure 4c) but at 16:00 it was only 5 km to the west of it (Figure 4d). This sudden and transient increase on low-level reflectivity by 16:00-16:10 is considered as a result of the direct influence of the approaching SBF over the plume, similar to the case studied by Hanley et al. (2013). The SBF continued to propagate eastwards and at 17:50 was still detectable on radar but displaced to the east of the fires (Figure 4e).

The pyroconvective plume was observed in low-level reflectivity at 500 m above the fires, as a V-shape pattern extending northwest of the buoyancy sources, driven by the flow at that level (Figure 4, Figure 6). Two independent plumes were identified as departing from each buoyancy source, but merged downwind of them due to fires proximity (Figure 4, Figure 6). The plume of the southwest fire looked discontinuous due to strong clutter cancelation effects over the mountainous area located to the northwest of the buoyancy source. This can be seen with the C/CL radar (Figure 6) but also with the A/PG radar (Figure 7). Still, it can be observed a larger

magnitude of the reflectivity in the area of the plume slightly downwind of the fire, close to "L" at 16:30 (Figure 6a), when compared to the value observed at 16:00 (Figure 4d). At 16:40 an even larger reflectivity (41, 5 dBZ) was observed in the same area of the plume (Figure 6b).

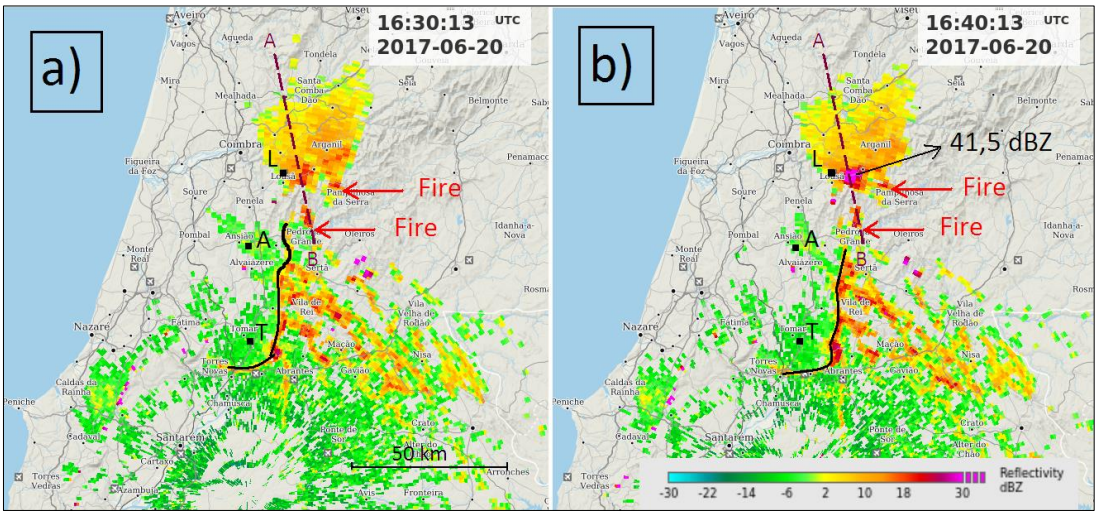

Figure 6- PPI of reflectivity, 0.1° tilt, 20 June 2017, C/CL radar. (a) 16:30 UTC, (b) 16:40 UTC. "L" Lousã, "A" Ansião, "T" Tomar AWS's. Buoyancy sources are represented by red arrows and "FIRE". "AB" dashed segment in (a) represents transect of the vertical section represented in Figure 7(c). "41,5 dBZ" highlights large magnitude reflectivity.

A sequence of static vertical sections of reflectivity and ρhv illustrates the vertical growth of the smoke plume and its transition to a pyrocumulus cloud (Figure 7). At 16:00 the smoke plume top was at 6000-7000 m a.m.s.l., as in previous observations (not shown). Its reflectivity (Figure 7a, upper) was produced by pyrometeors (ρhv ≤ 0.7, greenish colors in Figure 7a, lower), without significant condensation. This was consistent with the observed LFCV (Level of Free Convection from virtual temperature) at 5600 m a.m.s.l. at 12:00 (Figure 2). However, as the SBF started to influence the plume, it was noticed a vertical expansion of it, so that by 16:30 the top was at 9000 m (Figure 7b, upper). By then there were signs of condensation/glaciation in upper levels (ρhv > 0.7; yellowish colors in Figure 7b, lower). At 16:50 its top was at 12500 m, reflectivity attained 50.5 dBZ in the convective core (3500 m a.m.s.l.), 40 dBZ at 1200 m altitude (Figure 7c, upper) and condensation arrived at low levels (Figure 7c, lower). The hydrometeor algorithm (not shown) classified as *rain*, *graupel* and *hail* large fractions of the pyrocumulus transect, suggesting that some precipitation may have reached ground levels but there was no ground truth to verify it. This pyrocumulus peaked at 13000 m by 17:00 (not shown) and started to lose buoyancy afterwards, lowering as observed at 17:20 (Figure 7d). A photograph taken from Coimbra, 25 km to the west, shows the outstanding pyroCu at 16:48 (Figure 8).

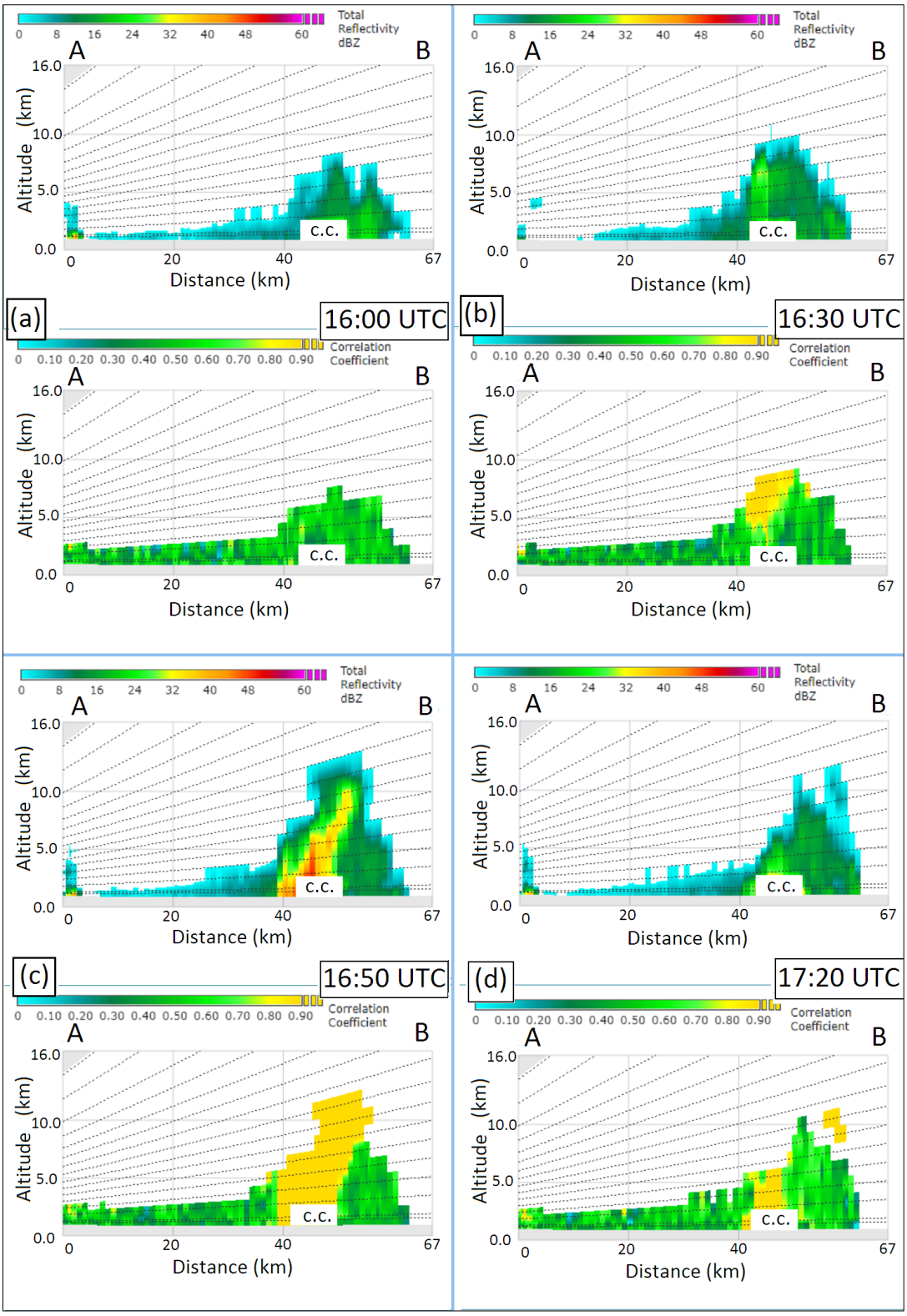

Figure 7- Vertical sections of reflectivity ((a), (b, (c), (d), upper) and of ρhv ((a), (b), (c), (d), lower), 20 June 2017, A/PG radar. (a) 16:00 UTC, (b) 16:30, (c) 16:50 UTC, (d) 17:20 UTC. Horizontal axis with distance marks every 20 km up to 67 km. Vertical axis with distance marks every 5 km up to 16 km."C.C." white rectangle depicts the area contaminated by strong clutter cancelation. Greenish colors represent smoke, yellowish colors represent condensation/glaciations of pyrometeors. (see figures 4 and 6 for reference of the transect location).

Figure 8- Photograph of the pyrocumulus cloud taken from Coimbra, at 16:48 UTC, 20 June 2017 (note: confront with Figure 7c). Extracted fromViegas et al. (2017).

4. References:

Balakrishnan, N.; Zrnic, D.S. Use of Polarization to Characterize Precipitation and Discriminate Large Hail. J. Atmos. Sci. 1990, 47, 1525–1540. https://doi.org/10.1175/1520-0469(1990)047<1525:UOPTCP>2.0.CO;2

Fromm, M. D., R. H. D. McRae, J. J. Sharples, and G. P. Kablick III, 2012: Pyrocumulonimbus pair in Wollemi and Blue Mountains national parks, 22 November 2006. Aust. Meteor. Oceanogr. J., 62, 117–126, *https://doi.org/10.22499/2.6203.001*.

Hanley, D., Cunningham, P., Goodrick, S. 2013. Interaction between a wildfire and the sea-breeze front. In Qu, John J., Sommers, William T., Yang, Ruixin; Riebau, Allen R. (eds.). Remote sensing and modelling applications to wildland fire. Beijing, China: Tsinghua University Press and New York Spirnger. Pgs. 81 - 98

Jones, T.A.; Christopher, S.A. Satellite and radar observations of the 9 April 2009 Texas and Oklahoma grassfires. Bull. Am. Met. Soc. 2010, 91, 455–460. https://doi.org/10.1175/2009BAMS2919.1

LaRoche, K.T.; Lang, T.J. Observations of Ash, Ice, and Lightning within Pyrocumulus Clouds Using Polarimetric NEXRAD Radars and the National Lightning Detection Network. Mon. Weather Rev. 2017, 145, 4899–4910. *https://doi.org/10.1175/MWR-D-17-0253.1*.

Lang, T.J.; Rutledge, S.A.; Dolan, B.; Krehbiel, P.; Rison, W.; Lindsey, D.T. Lightning in Wildfire Smoke Plumes Observed in Colorado during Summer 2012. Mon. Weather Rev. 2014, 142, 489–507. https://doi.org/10.1175/MWR-D-13-00184.1.

McCarthy, N.; Guyot, A.; Dowdy, A.; McGowan, H. Wildfire and Weather Radar: A Review. J. Geophys. Res. 2019, 124, 266–286. https://doi.org/10.1029/2018JD029285

Miller, S.T.K., Keim, B.D., Talbot, R.W., Mao, H. Sea breeze: Structure, forecasting, and impacts.. Reviews of Geophysics, Volume 41, Issue 3

Peterson, D. A., E. J. Hyer, J. R. Campbell, J. E. Solbrig, and M. D. Fromm, 2017: A conceptual model for development of intense pyrocumulus in western North America. Mon. Wea. Rev., 145, 2235–2255, *https://doi.org/10.1175/MWR-D-16-0232.1*.

Pielke, R.A., Song, A., Michaels, P.J., Lyons, W.A., Arritt, R.W.. The predictability of sea-breeze generated thunderstorms. Atmósfera, vol. 4,. núm. 2, abril, 1991, pp. 65-78. Universidad Nacional Autónoma de México. Distrito Federal, México

Pinto, P.; Silva, A.P.; Viegas, D.X.; Almeida, M.; Raposo, J. Influence of Convectively Driven Flows in the Course of a Large Fire in Portugal: The Case of Pedrógão Grande. Atmosphere 2022, 13, 414. https://doi.org/10.3390/atmos13030414

Srivastava, R. A model of intense downdrafts driven by the melting and evaporation of precipitation. J. Atmos. Sci. 1987, 44, 12, 1752–1774. https://doi.org/10.1175/1520-0469044<1752:AMOIDD>2.0.CO;2

Viegas, D.X.; Almeida, M.; Ribeiro, L.; Raposo, J.; Viegas, M.T.; Oliveira, R.; Alves, D.; Pinto, C.; Humberto, J.; Rodrigues, A.; et al. O Complexo de Incêndios de Pedrógão Grande e Concelhos Limítrofes, Iniciado a 17 de Junho de 2017. ADAI-CEIF, Coimbra. 2017 (In Portuguese). Available online http://www.portugal.gov.pt/donwload-ficheiros/ficheiro.aspx?v=3bb97773b-59fb-4099-9de5-a22fdcad1e3b (accessed on 12 November 2021).